Design Principles and Performance Evaluation of a Novel Axial Flux Consequent-Pole Resolver

Vahid Naeini*, Assistant professor

Department of Electrical Engineering, Malayer University, Malayer, Iran.

vnaeini@malayeru.ac.ir

Abstract

In this paper, a new structure for an axial flux consequent pole resolver (AFCPR) with concentrated windings on the stator is presented and analyzed. In this proposed design, the magnetic poles of the rotor are created by symmetrical saliences in the ferromagnetic core of the rotor instead of using permanent magnets, arranged in an alternating pattern with the same magnetic direction. By applying current to the concentrated windings of the stator along the axial direction, a suitable flux density is generated to produce iron poles. The main innovation of this structure lies in the elimination of permanent magnets and the simple, lightweight, and robust design of the rotor, which enhances reliability in position and speed estimation. The performance of the proposed resolver has been examined using two different winding patterns to generate sinusoidal and cosine signals, in order to analyze their effects on improving functional harmonics and reducing position error. Three-dimensional simulations using the 3D Finite Element Analysis (3D-FEA) method demonstrate that this resolver has adequate accuracy in position estimation and that the selection of the appropriate winding pattern can significantly improve positioning accuracy.

Keywords: axial flux consequent pole resolver (AFCPR), rotor position estimation, 3D Finite Element Analysis.

1. Introduction

In the operation and control of many electric machines, rotor position and speed sensors play a crucial role in the control loops of various applications across industries, for which a variety of sensors can be utilized. Among the different position detection sensors, optical sensors are widely established and recognized; however, their performance is influenced by environmental factors such as temperature, smoke, dust, and vibration [1]- [4]. Another type of rotor position sensor is the Hall Effect sensor (HS), which is useful in many applications due to its reliance on magnetic field properties [5]- [8]. Nevertheless, it is sensitive to precise flux density and may not be suitable for high-resolution applications. Recently, resolvers have gained increased attention as position sensors for electric machines due to their inherent advantages, such as robust structure, suitable size, capability to operate in contaminated environments, and ability to function across a wide range of frequencies, temperatures, and vibrations. These features have led to an increasing

* Corresponding author
Tel.: +98 81 33339881; fax: +98 81 32355465.

E-mail address: vnaeini@malayeru.ac.ir (V. Naeini).

application of resolvers in sensitive industries such as aerospace, automotive, and robotics [9]-[33]. To provide a foundational understanding, resolvers operate as rotary transformers that measure angular position by utilizing electromagnetic coupling between the rotor and stator windings. These systems typically employ radial flux designs, where the magnetic flux flows perpendicular to the axis of rotation. Radial flux resolvers are widely recognized for their robustness, reliability, and precision; however, their larger axial dimensions can pose challenges for integration into compact systems. In contrast, axial flux resolvers, as reported in the literature, present a promising alternative by offering a more compact geometry and potentially higher efficiency. Their design enables magnetic flux to flow parallel to the axis of rotation, which reduces axial length and allows for improved space utilization. Despite these advantages, axial flux designs are often limited by increased design complexity and manufacturing challenges.

However, challenges such as structural complexity, winding type, and production costs have led to extensive research focused on the development and optimization of resolver structures. In early versions, resolvers utilized wound rotors that required the injection of excitation signals through a rotating transformer [9]-[16]. This resulted in increased dimensions, complexity, and costs of the device, as a rotating transformer was needed to power these windings. Consequently, the presence of an internal rotating transformer in the resolver core led to larger dimensions and additional costs. In another type of resolver, the variable reluctance structure eliminates the excitation winding from the rotor and places it on the stator, resulting in a simpler design [17]-[23]. On the other hand, the Permanent Magnet Resolver (PM-Resolver) is a new position sensor that uses PM poles and operates without an input signal. Due to advantages such as a compact and lightweight structure and reduced winding usage, PM-resolvers have recently gained considerable popularity in various industrial applications [24]-[26]. However, the use of permanent magnetic materials faces challenges such as instability at high temperatures, demagnetization, high costs, and access limitations, which have imposed constraints in many industrial applications, negatively affecting their cost-effectiveness. Additionally, the gradual evolution of various resolver configurations indicates that axial flux resolvers (AFPM) are becoming increasingly popular compared to radial flux machines (RFPM) due to their distinct advantages and disk-like structures [27]-[33]. These machines allow for size reduction by increasing the number of poles, particularly for direct drive applications with low rotational speeds. Moreover, among the various types of resolvers, axial flux resolvers exhibit better performance under conditions of mechanical faults.

However, as previously described, it is essential to focus on reducing costs, simplifying the structure, and, of course, enhancing the reliability of resolvers. To minimize the use of permanent magnet (PM) materials without compromising magnetic flux density, the Consequent Pole (CP) structure presents an attractive option where all permanent magnetic poles in iron-core machines are replaced [34]-[36]. Machines with a consequent pole structure have been widely used and investigated for various applications, facing numerous challenges to overcome in their design to remain competitive in terms of overall machine performance. Therefore, this paper proposes an axial flux consequent pole resolver (AFCPM) that does not utilize permanent magnetic materials. In this structure, as the name suggests, the magnetic poles are generated by saliences in the ferromagnetic rotor core with the same magnetic direction arranged in an alternating pattern. In this resolver, the desired iron poles of the rotor are produced using a DC field winding on the stator core, eliminating the need for permanent magnetic poles in the rotor structure. By injecting appropriate and selective current into the DC field winding, a suitable magnetic field density is generated on the rotor's iron poles. Consequently, the air gap flux density can be adjusted, making the machine highly desirable for various applications with regulated output voltage. The key advantage of this machine lies in its simple, cost-effective design, particularly its robust one-piece

rotor, which is well-suited for high-speed applications. This rigid rotor structure enhances performance by minimizing the effects of external forces on the rotor, while also ensuring high reliability under fault conditions. Therefore, these factors make this resolver an optimal choice for many applications.

Furthermore, one of the main challenges in the operation of resolvers is the presence of voltage harmonics in the sinusoidal and cosine signals, which leads to errors in position and speed detection. The main source of these harmonics is due to the variety of signal winding patterns. In this study, two different winding patterns have been investigated to examine their effects on reducing distortion and improving position accuracy. The performance analysis of this proposed structure has been conducted using the three-dimensional Finite Element Method (3D-FEM) to thoroughly evaluate the magnetic field accuracy and the electromagnetic performance of the resolver. In the subsequent section, a detailed design of components, key parameters, and the topology of the structure will be presented, focusing on the replacement of permanent magnetic poles with iron poles.

In the following sections of this article, the proposed resolver's structure and topology will be described in detail in Section 2. Section 3 will examine the electromagnetic operating principles of the resolver and the method of generating sinusoidal and cosine signals using two different winding patterns. Finally, in Section 4, the results of the three-dimensional simulations (3D-FEM) will be presented, along with an analysis and comparison of the resolver's performance and positioning accuracy. Section 5 will summarize the findings and provide recommendations for future research.

2. Topology Description of the proposed AFCPR

The various components of the schematic structure of an axial flux consequent pole resolver (AFCPR) are illustrated in Figure 1. As shown in Figure 1, this resolver employs a symmetrical configuration relative to the central stator core, with the stator core positioned between two coaxial disc rotors. These two rotor discs are mounted on a common shaft, allowing for their simultaneous and symmetrical rotation. The dual-sided rotors consist of a series of ferromagnetic iron poles made of electrical steel (such as silicon sheets), which are alternately positioned in the north and south magnetic pole locations. These poles are integrated as protruding cores within the rotor structure and are axially and symmetrically aligned with respect to the central stator, extending along the radial axis of the device.

The key feature of this structure compared to conventional resolvers is the elimination of permanent magnets and their replacement with consequent poles. In this design, the magnetic flux required to excite the rotor poles is generated through a DC field winding installed on the stator. This created magnetic field symmetrically flows into the rotors, resulting in the formation of alternating magnetic poles (north and south) in the rotor, without the need for permanent magnetic materials. This design not only simplifies the structure and reduces costs but also leads to a decrease in rotor weight, increased mechanical strength, and improved thermal stability of the sensor, making it highly suitable for industrial applications under harsh operating conditions.

The stator core of the AFCPR resolver is designed to include two distributed signal windings for generating sinusoidal and cosine signal output voltages. These windings are symmetrically placed in the radial slots on both sides of the disc stator, arranged so that their spatial distribution is configured to produce induced voltage waveforms that have orthogonal phases (90 degrees of electrical phase difference) with respect to the angular position of the rotor. This feature enables precise extraction of the angular position of the shaft and ensures accurate and high-resolution operation of the resolver. The signal windings located at upper and lower sides of the stator core can be connected electrically in series or parallel, which in this paper are connected in series. At the center of the stator, there is an excitation winding responsible for generating the primary magnetic field of the device. This winding is powered by a DC voltage source and plays a crucial role in providing the magnetic flux necessary for the formation of the iron poles in the rotor discs. The mechanical structure of this winding is designed so that the produced flux flows axially toward the two rotors, ultimately creating a closed path for the magnetic flux through the rotor, air gap, and stator.

The iron poles in the two rotor discs are designed as mechanical protrusions made of ferromagnetic materials. These poles do not have any internal field source (such as permanent magnets) and are magnetized solely by the flux generated from the DC field winding. By adjusting the current supplied to the DC field winding, the magnetic flux density produced in the rotor poles can be dynamically controlled. This feature provides high flexibility in adapting the resolver's performance to various operating conditions and enables voltage output adjustment and system performance optimization. In fact, the AFCPR resolver, by utilizing the DC field winding to supply the magnetic pole flux, eliminates the need for expensive and temperature-sensitive permanent magnetic materials. This not only reduces manufacturing costs and increases reliability under harsh environmental conditions but also simplifies the production process and enhances the system's recyclability and maintainability. Therefore, this structure can serve as an effective and suitable alternative to conventional resolvers that use permanent magnets.

In Figure 2, the two main operational states of the AFCPR resolver are illustrated: the first state is when no current is injected into the DC field winding, and the second state is when DC current is applied to the field winding, generating a magnetic field within the machine core. These two conditions effectively demonstrate the magnetic behavior of the system. In the unexcited state (zero current), according to Ampère's law, no magnetic force is generated in the core environment, resulting in the absence of any magnetic flux in the magnetic path between the rotor, stator, and rotor. This condition renders the system inactive in terms of producing output position signals, as there is no electromagnetic force available to induce voltage in the sinusoidal and cosine signal windings.

In the second state, when direct current is applied to the excitation field winding, an axial magnetic field is generated at the center of the stator, according to Ampère's law and Faraday's law. This field is flowed through the iron core of the device as magnetic flux, forming a closed loop of flux between the iron poles of the first rotor disc, the stator, and the second rotor disc. Consequently, the iron poles in each rotor disc alternate between north (N) and south (S) magnetic poles. The strength and direction of these poles are entirely dependent on the amplitude of the current injected into the field winding. As the excitation current increases, the magnetic flux density also rises, which directly leads to an increase in the amplitude of the induced voltage in the output position

windings (sinusoidal and cosine signal). Since the generated magnetic flux is linearly proportional to the excitation current, the magnetic performance of the resolver can be finely tuned with high precision. This dynamic control of the magnetic field allows for adaptable operation in various applications, enhancing the resolver's versatility and performance in measuring angular positions accurately.

The ability to adjust the magnetic flux density is a crucial feature in precision positioning applications. In various operating conditions where errors in angular position detection may occur (due to noise, electromagnetic interference, or temperature variations), fine-tuning the excitation current allows for dynamic reduction of the resolver's operational errors and improves output accuracy. In summary, the flexible structure of the AFCPR enables the control of not only the density of the magnetic poles through field current management but also actively maintains the accuracy and stability of the resolver's positioning performance under varying operational conditions.

This model could not only provide a simpler yet effective representation of the magnetic flux paths and key magnetic interactions within the core, but also clarify the relationship between excitation current, flux density, and induced voltages, thereby facilitating the process of initial design and optimization. Also, a magnetic equivalent circuit model will be developed to complement the results of the 3D FEA and further optimize the proposed structure. This approach will enable better visualization of magnetic flux distribution, faster parameter estimation, and greater flexibility in the design process.

3. The operation principle of the proposed AFCPR resolver.

The operation and topology of the proposed AFCPR resolver bear a strong resemblance to that of an Axial Flux Permanent Magnet Resolver in terms of working principles. In fact, permanent magnet resolvers are a type of two-phase synchronous generator that produce angular position signals based on electromagnetic induction. In these structures, instead of feeding the rotor windings with an excitation current source, permanent magnetic poles are used to generate a constant magnetic field. This constant field induces positional voltages in the stator sensor windings. However, in the proposed AFCPR resolver, as previously explained, permanent magnetic poles are not used; rather, the necessary magnetic field for system excitation is provided through a concentrated DC excitation winding embedded in the center of the stator core. By applying direct current, this winding alternates the iron poles mounted on the rotor discs between north (N) and south (S) poles. Therefore, the AFCPR resolver, without the use of permanent magnetic materials, enables the generation of a controllable and adjustable magnetic field.

When the magnetic field is generated through the excitation winding, the mechanical rotation of the rotor causes a continuous change in the angular position of the iron poles relative to the receiving windings in the stator. In this case, according to the operational principles of resolvers, induced voltages with sinusoidal and cosine signal functions are generated in the two output windings of the stator concerning the angular position of the rotor. More specifically:

- The first stator winding induces a voltage proportional to the function $\cos(\theta)$.
- The second winding induces a voltage proportional to the function $\sin(\theta)$.

where θ represents the instantaneous angular position of the rotor relative to the stator. Using these two orthogonal signals, the exact angular position of the rotor can be extracted and converted into a digital signal through vector analysis methods or resolver-to-digital converters. This unique structure, utilizing controllable electromagnetic excitation instead of permanent magnets, not only enhances flexibility and operational accuracy under varying environmental and operational conditions but also enables dynamic performance improvement and reduction of angular position detection errors in the system.

The disc-shaped structure of the stator and rotor cores in the AFCPR resolver, along with the presence of asymmetric protrusions on the surfaces of the rotor discs, results in a non-uniform and anisotropic distribution of the magnetic field within the machine. This inhomogeneity in the field is particularly pronounced in areas close to the air gap and at the boundary between the iron poles and the stator slots, leading to complex behavior in terms of magnetic flux. Consequently, accurate modeling of this type of structure, especially during the electromagnetic analysis process, necessitates the use of three-dimensional finite element analysis (3D-FEA) methods to precisely predict the actual behavior of the field, induced voltages, flux density, and their distribution throughout the volume of the machine.

Since the air gap of the machine is non-uniform and asymmetric due to the specific geometric shape of the rotor discs, simplifications such as axial symmetry or radial periodicity cannot be utilized. Consequently, modeling only a portion of the machine's geometry is insufficient; the entire three-dimensional geometry of the resolver must be comprehensively modeled and analyzed. This requirement leads to an increase in computational volume, particularly during the meshing stage. In the 3D geometry meshing process, special attention is paid to the air gap region, as significant changes in the magnetic field occur in this area, necessitating greater accuracy in calculating the field gradients and flux density. Therefore, the mesh density in this region is considered to be very fine and compact, which significantly increases the number of mesh elements and, as a result, raises the computational time and resources needed to solve the model.

The main dimensions and design parameters of the proposed resolver are presented in Table 1, which includes the geometric specifications of the rotor discs, stator core, number of poles, slots, air gap length, and winding parameters. To examine the performance validity of the proposed structure and analyze the impact of the winding pattern on the quality of the output voltages and field density, two different winding design patterns have been evaluated:

- Single Layer Pattern with 32 slots in the stator.
- Double Layer Pattern with 16 slots in the stator.

These two winding patterns are schematically illustrated in Figure 3. It is worth noting that, despite the differences in the number of stator slots and the arrangement of the phases, all other geometric and dimensional parameters of both resolvers are considered identical. Additionally, in both structures, the windings of each phase are connected in series on both sides of the stator core to enhance the magnetic field generated at the center of the core and simultaneously improve operational characteristics. Analyzing and comparing the results obtained from these two structures provides valuable insights into the impact of winding topology on output accuracy, the

waveform of the induced voltage, flux density, and the electromagnetic efficiency of the resolver, thereby aiding in the selection of the most optimal configuration for practical applications.

The general purpose sizing equation and the main dimensions for axial flux machines has the following form. The phase back EMF, e_{ph} , is defined as:

$$e_{ph}(t) = 2\pi f . K_w . N_{ph} . B_g . A_p Sin(wt) \quad (1)$$

where, f, K_w, N_{ph}, w and B_g are power source frequency, winding coefficient, phase turn number, angular speed and the peak of pole flux density. The pole cross section for this machine, A_p, is calculated as:

$$A_p = \alpha_p \frac{\left({D_o}^2 - {D_{of}}^2\right)\pi}{4p} = \alpha_p \frac{\left({D_{if}}^2 - {D_i}^2\right)\pi}{4p} \quad (2)$$

Where p is poles number, α_p is ratio of pole arc to pole pitch (pole span), D_o, D_i , D_{of} and D_{if} are outer and inner radiuses of machine and dc field winding that are shown in figure 4.

Also, B_g, is the magnetic flux density in the air gap at the surface of the rotor's electrical magnets resulting from the field winding current. It is dependent on the field winding current and can be calculated from the equivalent magnetic circuit. The figure 5 shows 3D magnetic equivalent circuit of the pole pair of AFCPR. In this figure R_{rp}, R_{ry}, R_{st} and R_g, are the reluctances of the rotor pole and yoke, the stator tooth and the air gap respectively. As shown in this figure, the flux per pole is flowed from the stator core to the rotor throughout the air gap.

Therefore as shown in figure 5, the flux per pole (φ_P) is calculated as:

$$\varphi_P = \frac{N_f I_f}{2\mathcal{R}_{st} + 2\mathcal{R}_{ry} + 4\mathcal{R}_{rp} + 4\mathcal{R}_g} \quad (3)$$

And thus, the magnetic flux density, B_g, is calculated using the following relationship:

$$B_g = \frac{\varphi_P}{A_p} = \frac{N_f I_f}{(2\mathcal{R}_{st} + 2\mathcal{R}_{ry} + 4\mathcal{R}_{rp} + 4\mathcal{R}_g) A_p} = \frac{N_f I_f}{R_m A_p} \quad (4)$$

Where N_f is the number of turns of the DC field winding in the stator, I_f is the field winding current, and R_m is the total magnetic reluctance of the path. It should be noted that $B_g$behaves similarly to the flux density of a permanent magnet for the electromagnetic magnet.

Herein by measuring the induced voltages in each phase winding, the air-gap flux per pole is calculated as below:

$$e_{ph} = \frac{d\lambda_{ph}}{dt} \Rightarrow \quad \lambda_{ph} = \int e_{ph} dt \quad (5)$$

where λ_{ph} and N_{ph} are the linkage flux per phase and the number of turn of each phase winding respectively. Therefore, the linkage flux of Sin and Cos winding are derived from the voltage waveforms as

$$\begin{cases} e_c(t) = \frac{d\lambda_c(t)}{dt} = E_m Cos(wt + \theta_0) \\ e_s(t) = \frac{d\lambda_s(t)}{dt} = E_m Sin(wt + \theta_0) \end{cases}, \quad \begin{cases} \lambda_c(t) = \int e_c(t)\, dt = \lambda_m\, Sin(wt + \theta_0) \\ \lambda_s(t) = \int e_s(t)\, dt = \lambda_m\, Cos(wt + \theta_0) \end{cases} \tag{6}$$

It should be noted that Equation (6) was derived under ideal assumptions to simplify the theoretical analysis and provide a foundational understanding of the resolver's operation. However, practical factors such as rotor geometry, slotting, and consequent pole effects are known to introduce spatial harmonics, non-orthogonality, and signal distortion. In order to account for these challenges, a detailed 3D finite element analysis (FEA) is performed. This analysis incorporates all geometric details, including stator slotting and rotor consequent pole effects, while accounting for core saturation to simulate realistic operating conditions. This modeling approach enables a comprehensive evaluation of the potential impacts of these factors on the resolver's performance.

4. Simulation Results and Validation of the Proposed AFCPR

By employing the three-dimensional finite element analysis (3D-FEA) method, it is possible to precisely model and analyze the distribution of magnetic flux density across all regions of the resolver at any moment in time and at any rotor angular position. This method, by considering the complex and asymmetric geometry of the resolver structure, particularly the variable air gap and the non-uniform distribution of the magnetic field, enables highly accurate simulation of electromagnetic phenomena. Figure 6 illustrates a schematic representation of the 3D model, the geometry meshing, and the magnetic flux density distribution in various regions of the stator and rotor cores. In this figure, special attention has been given to fine meshing in areas adjacent to the air gap. This high mesh density is due to the sensitivity of the magnetic field behavior in this region and the necessity of accurately capturing its instantaneous and spatial variations, which is essential for obtaining precise results and minimizing simulation errors. From the results of the magnetic analysis, it is observed that the maximum magnetic flux density in the stator teeth is approximately 0.8 Tesla. This value is below the saturation threshold of the ferromagnetic material used in the core construction, indicating the effectiveness of the design in preventing magnetic saturation.

Figure 7 presents the induced voltage waveforms generated by the stator windings under the single-layer winding configuration (Case 1). These voltages are characterized as cosine (Cos(θ)) and sine (Sin(θ)) signals, which vary based on the rotor's angular position (θ). These signals are utilized for accurately determining the rotor's angular position through differential analysis or ratio calculations between the two output phases. Comparing the induced voltage signals obtained from finite element analysis with ideal reference signals (perfectly sinusoidal), it can be observed that, although the general waveform shape is preserved, there are deviations in both amplitude and waveform characteristics. These deviations are primarily caused by the following factors:

- Asymmetric air gap effects due to the disk-shaped rotor structure and uneven rotor protrusions.
- Non-ideal flux distribution across the teeth and slots of the stator.

- Presence of noise induced by flux edge effects and Lorentz forces in sharp geometric regions.

These irregularities in the output signals lead to the generation of high-frequency components or subharmonic distortions in the induced voltage. Such distortions may introduce unwanted noise into the rotor's angular position estimation process when these signals are converted into precise angular values. In other words, the position calculation error can increase due to disruptions in the induced voltage and the non-uniformity of the magnetic field. Therefore, a detailed analysis of these distortions, along with the development of digital filters or corrective algorithms to mitigate their effects during the position estimation process, can significantly enhance the performance and accuracy of the angular measurement system based on the proposed AFCPR resolver.

Figure 8 illustrates the linkage flux profiles associated with the two-phase stator windings of the proposed AFCPR resolver. As a key component in the electromagnetic performance analysis of the machine, these linkage flux profiles play a critical role in determining the quality of the induced voltage signals and, ultimately, the accuracy of the position sensing system. As shown in this figure, the time-domain profiles of the linkage flux in each phase exhibit smooth, continuous, and well-organized waveforms, free from severe disturbances or undesirable oscillations caused by geometric or magnetic distortions. One key observation from these diagrams is the significant reduction in high-order harmonic effects, which are primarily induced by the uneven distribution of stator teeth, rotor slots, and the asymmetric air gap in the disk-shaped machine structure. This reduction highlights the effectiveness of the design choices, including the optimized geometry of the poles, the precise placement of the windings, and the appropriate selection of the number of slots and the winding method. These design considerations have successfully mitigated spatial harmonic components in the linkage flux profiles, ensuring improved electromagnetic performance and enhanced signal quality for the resolver system.

The elimination of these unwanted harmonic components not only improves the quality of the induced voltages and reduces signal distortions but also directly enhances the accuracy of rotor angle estimation. Since the rotor's angular position is calculated based on the analysis of the sinusoidal and cosine signal voltages induced in the stator windings, any distortion in these signals can lead to positioning errors. Consequently, based on the results presented in Figure 8, it can be concluded that the structural and electromagnetic design of the AFCPR resolver has been optimized to enable the extraction of clean, low-distortion linkage flux signals. This highlights the high potential of the proposed resolver for precise position measurement applications in motion control systems, robotics, and advanced electric drives.

Now, using the relationship below to determine the angle between the cosine and sine signals, the rotor position at any given moment can be calculated as follows:

$$\theta_r(t) = \text{Arg}(\lambda_s(t) + i\,\lambda_c(t)) = \text{Arg}(Cos(wt + \theta_0) + i\,Sin(wt + \theta_0)) \qquad (7)$$

The *Arg* function determines the angle between the cosine and sine signals as the phase angle of a complex number formed by these two signals. Figure 9 illustrates the identified rotor position $\theta_r(t)$ by the resolver in comparison with the actual rotor position. To better compare the results, the ideal rotor position is also plotted in this diagram. The rotor position error calculated by the

resolver is presented in Figure 10. As observed, rotor position determination results in an error of approximately 2.5 degrees during the rotor's 360-degree rotation, which is considered an acceptable outcome. The harmonic content of the rotor position error envelopes for the single-layer AFCPR, as shown in Figure 11, illustrates the frequency spectrum of the error signal. This analysis highlights the fundamental harmonic along with higher-order harmonics providing valuable insights into the potential error sources. With the change of the winding pattern to a double-layer configuration, this condition will be reassessed.

Figures 12 and 13 respectively illustrate the induced voltage waveforms of the cosine and sine phases, along with their corresponding flux linkages, for the second winding configuration: a double-layer arrangement with 16 stator slots. In this winding pattern, each stator phase consists of two separate coil layers symmetrically positioned on opposite sides of the stator core and connected in series. This winding pattern enhances the distribution of the magnetic field within the core and reduces the effects of unwanted magnetic interference. As observed in the figures, the induced voltage waveforms in the sine and cosine phases are significantly smoother and more regular compared to the single-layer configuration. This indicates that spatial distortions and higher-order harmonics caused by field non uniformity within the machine's internal structure are greatly minimized in this pattern. In particular, the flux linkage profiles presented in Figure 13 demonstrate more uniform slopes and softer temporal variations. This directly contributes to improved output signal quality and reduced magnetic noise, ultimately enhancing the accuracy of rotor angular position detection. Overall, the comparison between the results of the two winding configurations highlights that employing the double-layer arrangement with an optimized design can be considered an effective strategy to reduce spatial distortions, improve signal stability, and increase the performance accuracy of the proposed AFCPR resolver.

Using the relationship for determining the angle between the cosine and sine signals (Equation 7), the rotor position at each moment is obtained as depicted in the plot in figure 14. For better comparison, the ideal rotor position is also shown in this figure, and the rotor position estimation error by the resolver is presented in figure 15-a. As observed, the rotor position estimation results in an error of approximately 1 degree over the 360-degree rotation of the rotor, which indicates an improvement compared to the previous single-layer winding configuration.

For a more qualitative analysis, the difference between the calculated rotor position and the ideal value is illustrated as an angular error plot in figure 15-b. Based on this figure, it can be observed that the angular error remains approximately 1 degree across most points of the rotor's 360-degree cycle. This error shows a significant reduction compared to the previous single-layer winding configuration, demonstrating an improved performance of the angular position extraction algorithm in the double-layer winding setup. The harmonic content of the rotor position error envelopes for the double-layer AFCPR, as shown in Figure 16, illustrates the frequency spectrum of the error signal. As demonstrated by this figure, the harmonic profile of the error signal exhibits superior performance compared to the single-layer configuration.

These results confirm that the optimized winding structure, combined with precise three-dimensional meshing and proper control of magnetic excitation parameters, effectively reduces the error in rotor position estimation. Such accuracy is crucial for applications requiring precise

position detection in dynamic conditions or environments with external noise, highlighting the high potential of the proposed AFCPR structure for use in high-precision position sensing systems.

To enhance the practical significance of the proposed axial flux resolver topology, relevant experimental studies reported in the literature have been reviewed. Reference [27] provides a detailed investigation of a similar axial flux resolver structure, covering its design, optimization, fabrication, and experimental validation. The experimental results from [27], presented in Figure 17, demonstrate the feasibility of axial flux resolver structures in real-world conditions, achieving a rotor position error of approximately 4 degrees. In contrast, the resolver proposed in this study achieves a significantly improved position error of approximately 1 degree, as shown in Figure 15. This comparison underscores the effectiveness of the proposed design and optimization methodology and highlights its potential for achieving superior performance compared to existing experimental designs.

5. Discussion

The results obtained from the 3D simulation of the proposed AFCPR resolver demonstrate the desirable performance of this structure in extracting the roter's angular position with acceptable accuracy. As observed in the analysis of the induced voltages and flux linkages, the optimized winding design and the use of a DC excitation coil concentrated at the center of the stator core, instead of a permanent magnet, provide greater flexibility in controlling the magnetic flux amplitude. Moreover, this approach allows for better adaptability to different operational conditions. A comparison between the single-layer and double-layer winding structures revealed that the double-layer configuration, with a reduced number of slots, leads to a more balanced distribution of the magnetic field and a reduction in spatial harmonics. This, in turn, results in sinusoidal cosine and sine induced voltages with lower distortion. Such improvements have a direct impact on the reduction of angular error in the extracted position. Specifically, in the double-layer configuration, the rotor's angular position error was limited to approximately 1 degree, representing a significant improvement over the initial single-layer winding design.

On the other hand, the use of 3D-FEM for accurate modeling of the structure, particularly in the asymmetric air gap region and non-uniform teeth, has been essential and unavoidable. This precise modeling enables the observation of localized effects on flux density distribution and the dynamic behavior of the resolver, demonstrating that the proposed design does not experience magnetic saturation within the specified operating range and remains within the safe working limits of ferromagnetic materials. Overall, it can be concluded that the proposed AFCPR structure, utilizing adjustable electromagnetic excitation, has the potential to replace permanent magnet resolvers. Furthermore, with additional optimization in mechanical structure, winding design, and angular extraction algorithms, it can serve as a precise, cost-effective, and environmentally adaptable option for industrial and automotive applications. This structure also paves the way for the development of resolvers with intelligent and adaptive control in future electromechanical systems.

The promising simulation results of the proposed AFCPR resolver highlight its potential for precise angular position extraction. To further enhance the performance of the proposed AFCPR resolver, future work will prioritize the optimization of the winding configuration and mechanical

structure to reduce voltage harmonic distortions and improve angular positioning accuracy. Specifically, refining the double-layer winding design and optimizing the slot configuration will be critical in achieving a more balanced magnetic field distribution, minimizing spatial harmonics, and generating sinusoidal induced voltages with lower distortion. These improvements are expected to directly contribute to the reduction of angular error in position measurement.

6. Conclusions

In this study, an innovative design of an axial flux resolver with consequent poles (AFCPR) was introduced and analyzed without the use of permanent magnets. The resolver design eliminates permanent magnetic elements and replaces them with a DC excitation coil concentrated on the stator, enabling the generation of a controllable magnetic field. This feature not only simplifies the structure and reduces production costs but also enhances flexibility in field intensity control, providing greater adaptability under varying operating conditions. Key advantages of the proposed resolver include its lightweight rotor, elimination of permanent magnets, and high reliability, making it a suitable option for industrial, automotive, and precision positioning applications. In this paper, the operating principles of the AFCPR resolver and its magnetic field distribution were first examined. Subsequently, using 3D finite element analysis, the magnetic flux density distribution, phase-induced voltages, and flux linkages were analyzed. Simulations demonstrated that the proposed structure performs well in terms of avoiding magnetic saturation, achieving balanced field distribution, and generating induced voltages, showing good alignment with theoretical expectations. Additionally, a comparison of two different stator winding configurations (single-layer and dual-layer) revealed that altering the winding arrangement significantly reduces spatial harmonics and improves the accuracy of rotor angular position extraction. Specifically, in the double-layer configuration, the position extraction error was limited to approximately 1 degree, representing a notable improvement over the initial single-layer design. In summary, the proposed AFCPR resolver, with its simplified design, lower cost, adjustable magnetic field, and precise performance, has the potential to serve as a suitable replacement for permanent magnet resolvers in many forward-looking industrial applications. Moreover, it provides a robust foundation for further development and integration into intelligent positioning systems of the future.

References

[1] Zhao J., Qu W., Cai N., et al, "Measurement Error Analysis and Compensation for Optical Encoders: A Review," IEEE Transactions on Instrumentation and Measurement, vol. 73, pp. 1-30, 2024, https://doi.org/10.1109/TIM.2024.3417589

[2] Shen P., "Advancements in integrated circuit encoders: design, optimization, and applications in high-precision control systems," 2nd International Conference on Mechatronic Automation and Electrical Engineering (ICMAEE 2024), China, 2024, pp. 525-530, https://doi.org/10.1049/icp.2024.4576

[3] Mao Y., Tong J., Chin Z., et al, "Transmission-error- and vibration-based condition monitoring of gear wear with contaminated lubricant", Wear, Vol 523, 2023, https://doi.org/10.1016/j.wear.2023.204760.

[4] Gurauskis D., Kilikevičius A., Borodinas S., "Experimental Investigation of Linear Encoder's Subdivisional Errors under Different Scanning Speeds", Applied Sciences, Vol. 10(5), March 2020, https://doi.org/10.3390/app10051766.

[5] Sorial R. R., Soliman M. H., Hasanien H. M., et al, "A Vector Controlled Drive System for Electrically Power Assisted Steering Using Hall-Effect Sensors," in IEEE Access, vol. 9, pp. 116485-99, 2021, https://doi.org/10.1109/ACCESS.2021.3105609.
[6] Akrami M., Jamshidpour E., Baghli L., et al, "Application of Low-Resolution Hall Position Sensor in Control and Position Estimation of PMSM—A Review", Energies, Vol. 17, No. 17, 4216, 2024, doi:10.3390/en17174216.
[7] Fernandez D., Fernandez D., Martinez M., et al, "Resolver Emulation for PMSMs Using Low Cost Hall-Effect Sensors," in IEEE Transactions on Industry Applications, vol. 56, no. 5, pp. 4977-4985, Sept.-Oct. 2020, https://doi.org/10.1109/ECCE.2019.8913229.
[8] Wu Z., Zhang J., Qian M., Zhou Q., "High-precision positioning of Hall probes for SCU magnetic field measurement", Nuclear Instruments and Methods in Physics Research Section A Accelerators Spectrometers Detectors and Associated Equipment, 1059(4), 2023, doi: 10.1016/j.nima.2023.169004.
[9] Celikel R., Boztas G., Aydogmus O., "An investigation on the position errors of resolvers designed in different structures: A review", Measurement, Vol. 218, 2023, https://doi.org/10.1016/j.measurement.2023.113186.
[10] Hu J., Lv K., Huang W. Lin, H., Wang D., "Temperature Measurement of PMSM Rotor Based on Wound-Rotor Resolver Reuse Technique," in *IEEE Transactions on Transportation Electrification*, vol. 11, no. 1, pp. 2415-2424, Feb. 2025, https://doi.org/10.1109/TTE.2024.3422662.
[11] Eesazadeh M. R., Nasiri-Gheidari Z., Tootoonchian F., "Innovative Winding and Tooth-Pole Configurations in the Development of Variable Reluctance Synchro", IEEE Sensors Journal. Vol. 25.(2), 2024, pp. 2494 – 2501, https://doi.org/10.1109/JSEN.2024.3507935.
[12] MohammadAli Rezayi, P., Tootoonchian, F., "Minimization of Space Harmonics for Fractional-Slot Windings of Multi-Speed Wound Rotor Resolvers", *Scientia Iranica*, 2025, https://doi.org/10.24200/sci.2025.64997.9238.
[13] Khazaee M., Tootoonchian F., "Comparing different configurations for rotary transformer of wound-rotor resolvers", Scientia Iranica, 2023; 30(2): 605-617. https://doi.org/10.24200/sci.2021.57984.5503.
[14] Mohammad-Yari M., Safari M. R., Alipour-Sarabi, R., et al. "Optimal winding selection for wound-rotor resolvers", *Scientia Iranica*, 2021; 28(6): 3429-3436. https://doi.org/10.24200/sci.2019.52439.2764.
[15] Zare F., and Nasiri-Gheidari Z., "Proposal of a 2DOF Wound-Rotor Resolver," in *IEEE* Sensors Journal, vol. 21, no. 17, pp. 18633-40, 2021, https://doi.org/10.1109/JSEN.2021.3089540.
[16] Tayfun G., "Sensitivity Analysis of Design Parameters in Limited-Angle Wound Rotor Resolver," in *IEEE Trans. on Instrum. and Measu.*, vol. 73, pp. 1-9, 2024, https://doi.org/10.1109/TIM.2024.3387971.
[17] Ran X., Zhao M., Shang J., "A novel axial reluctance resolver proposal and its winding configuration optimization using winding function method", Energy Reports, Vol. 8, No. 13, pp. 705-12, 2022, https://doi.org/10.1016/j.egyr.2022.08.094.
[18] Naderi P., "A novel Variable-Reluctance Resolver proposal and its performance analysis under healthy and eccentric cases", Mechatronics, Vol. 90, 2023, doi: 10.1016/j.mechatronics.2023.102948.
[19] Bahari M., Davoodi A., Saneie H., Tootoonchian F., et al, "A New Variable Reluctance PM-Resolver", IEEE Sensors Journal, vol. 20, no. 1, pp. 135 – 142, Jan. 2020, https://doi.org/10.1109/JSEN.2019.2941554.

[20] Lasjerdi, H., Nasiri-Gheidari, Z., “Improving the Performance of Variable Reluctance Resolver Against Short Circuit Using Physical Parameters”, *Scientia Iranica*, 2023, https://doi.org/10.24200/sci.2023.62539.7901
[21] Saneie H., Nasiri-Gheidari Z., Tootoonchian F., “Accuracy Improvement in Variable Reluctance Resolvers”, IEEE Trans. on Energy Conversion, vol. 34, no. 3, pp. 1563 – 1571, Sept. 2019. https://doi.org/10.1109/TEC.2019.2902630
[22] Salimi Moghaddam, G., Nasiri-Gheidari, Z., Alipour-Sarabi, R., “Field Reconstruction Modeling Method of a Linear Variable Area Resolver”, *Scientia Iranica*, 2024; https://doi.org/10.24200/sci.2024.64351.8889
[23] Soleimani M. R., Nasiri-Gheidari Z., Tootoonchian F., et al, “Optimal Design of Outer Rotor VR Resolver Based on MEC Model”, in *IEEE Sensors Journal*, vol. 25, no. 3, pp. 4440-7, 2025, https://doi.org/10.1109/JSEN.2024.3520339
[24] Bahari M., Tootoonchian F. and Mahmoudi A., "An Electromagnetic Design of Slotless Variable Reluctance PM-Resolver," in IEEE Transactions on Industrial Electronics, vol. 70, no. 5, pp. 5336-46, 2023. https://doi.org/10.1109/TIE.2022.3183333
[25] Sun L., Luo Z., Hang J., et al, "A Slotless PM Variable Reluctance Resolver With Axial Magnetic Field," in IEEE Transactions on Industrial Electronics, vol. 69, no. 6, pp. 6329-40, 2022. https://doi.org/10.1109/TIE.2021.3090704
[26] Ghandehari R., Naderi P. and Vandevelde L., "Performance Analysis of a New Type PM-Resolver in Healthy and Eccentric Cases by an Improved Parametric MEC Method," in *IEEE Transactions on Instrumentation and Measurement*, vol. 70, pp. 1-10, 2021. https://doi.org/10.1109/TIM.2021.3080388
[27] Nasiri-Gheidari Z., "Design, Analysis, and Prototyping of a New Wound-Rotor Axial Flux Brushless Resolver," in *IEEE Transactions on Energy Conversion*, vol. 32, no. 1, pp. 276-283, March 2017, https://doi.org/10.1109/TEC.2016.2604858
[28] Alemi-Rostami M., Alipour-Sarabi R., Rezazadeh G., et al, “Design Optimization of a Double-Stage Resolver”, IEEE Transactions on Vehicular Technology, vol. 68, no. 6, pp. 5407 – 5415, June 2019. https://doi.org/10.1109/TVT.2019.2909096
[29] Kong T., Sun L., Ding Y., et al, "Investigation of a Low-Power Consumption Decoding Method in an Axial Field Variable Reluctance Resolver," in *IEEE Transactions on Transportation Electrification*, vol. 11, no. 1, pp. 3433-41, 2025. https://doi.org/10.1109/TTE.2024.3442375
[30] Hajmohammadi S. and Nasiri-Gheidari Z., "Proposal of a Wound-Rotor PCB-Resolver," in *IEEE Transactions on Industrial Electronics*, vol. 71, no. 11, pp. 15122-29, 2024. https://doi.org/10.1109/TIE.2024.3376807
[31] KhajueeZadeh M. and Tootoonchian F., "Axial Flux Resolver Versus Radial Flux One From Fault Tolerability Point of View," in *IEEE Sensors Journal*, vol. 23, no. 17, pp. 19176-83, 2023. https://doi.org/10.1109/JSEN.2023.3296746
[32] Chang T. -W., Huang P. -W., Huang W. –C., et al, "Additive Manufacturing High Fault-Tolerant Axial Flux Variable Reluctance Resolver," in *IEEE Transactions on Magnetics*, vol. 59, no. 11, pp. 1-5, 2023. https://doi.org/10.1109/TMAG.2023.3290606
[33] Ran X., Shang J., Zhao M. et al, "Improved Configuration Proposal for Axial Reluctance Resolver Using 3-D Magnetic Equivalent Circuit Model and Winding Function Approach," in IEEE Transactions on Transportation Electrification, vol. 9, no. 1, pp. 311-21, 2023. https://doi.org/10.1109/TTE.2022.3199538.
[34] Ni Y., Wang P., Xiao B., et al, "Analytical Model of Consequent-Pole Flux Reversal Machine With Segmented Magnet Arrangement," in *IEEE Transactions on Magnetics*, vol. 61, no. 4, pp. 1-14, 2025. https://doi.org/10.1109/TMAG.2025.3545056

[35] Li F., Wang K., Li J., et al, "Electromagnetic Performance Analysis of Consequent-Pole PM Machine With Asymmetric Magnetic Pole," in *IEEE Transactions on Magnetics*, vol. 55, no. 6, pp. 1-5, 2019. https://doi.org/10.1109/TMAG.2019.2904948
[36] Naeini V., Ardebili M., "New axial flux PM less synchronous machine with concentrated DC field on stator", International Journal of Electrical Power & Energy Systems, Vol. 67, pp. 651-8, 2015. https://doi.org/10.1016/j.ijepes.2014.12.048

BIOGRAPHIES

Vahid Naeini was born in Hamedan, Iran, in 1984. He received the B.Sc. and M.Sc. degrees in electrical engineering from Shahed University, Tehran, Iran, in 2006 and 2009, respectively. He received the Ph.D. degree in electrical engineering from K. N. Tosi University of Technology, Tehran, Iran, in 2016. Since 2016, he has been an Assistant Professor with the Electrical Engineering at Malayer University, Hamedan, Iran. His main research interests include design, modeling and analysis of electrical machines and power transformers.

LIST OF FIGURES

Figure 12: Induced cosine and sine voltages of the resolver windings with double-layer winding configuration.

Figure 13: Flux linkage diagrams of the resolver windings with double-layer winding configuration.

Figure 14: Identified rotor position, $\theta_r(t)$, by the double-layer resolver compared to the actual rotor position.

Figure 15: the rotor position estimation error by AFCPR as a function of a) time and b) actual position of the double-layerresolver.

Figure 16: The harmonic content of the rotor position error envelopes for single-layer AFCPR.

Figure 17: Experimental results of the AFRs presented in reference [27], (a) the detected position versus the reference position and (b) the angular position error

LIST OF TABLES

Table 1. The parameters values and Dimensional information of AFCPR.

FIGURES AND TABLES

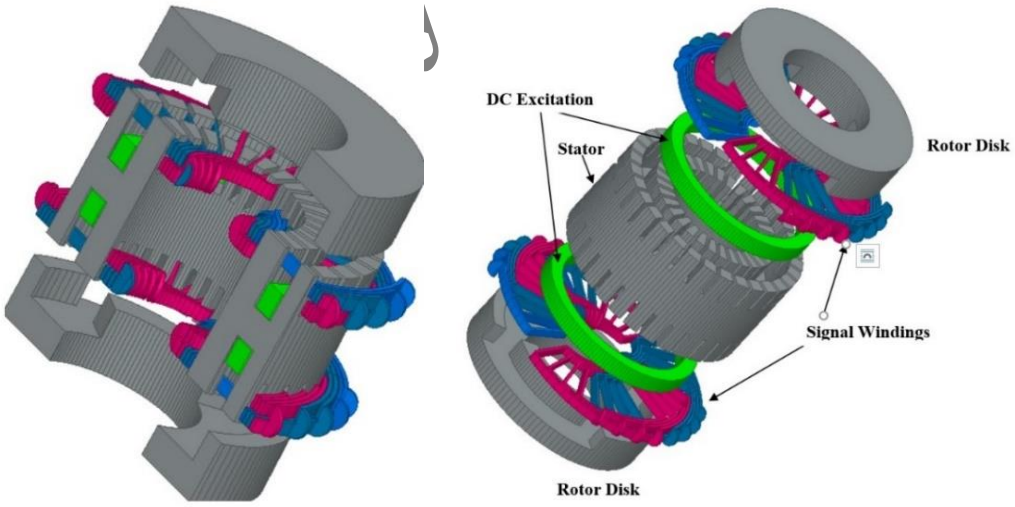

Figure 1: Schematic representation of the various components of the proposed AFCPR resolver.

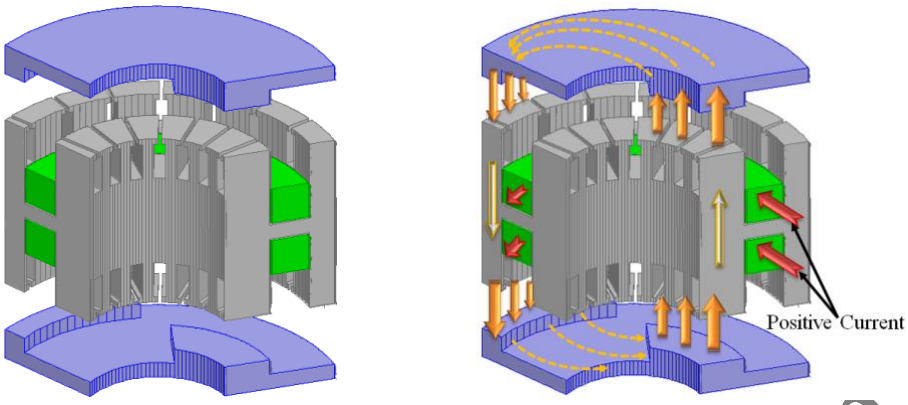

(a) (b)

Figure 2: Main flux path of the CPAFR with (a) zero, (b) positive DC current.

Table 1. The parameters values and Dimensional information of AFCPR.

Parameter	Symbol	Value
Stator and Rotor outer diameter	D_o	30^{mm}
Stator and Rotor inner diameter	D_i	15^{mm}
Stator Axial length	L_s	30^{mm}
rotor Axial length	L_r	12^{mm}
Stator slot deep	d_s	8^{mm}
DC excitation outer diameter	D_{of}	26^{mm}
DC excitation inner diameter	D_{if}	21^{mm}
Number of turn of each phase coil	N_s	400
Number of turns of DC excitation	N_f	200
Number of stator slots 1-layer/2-layer	n_s	32/16
Pole number	P	4
Rated current of DC excitation	A	3

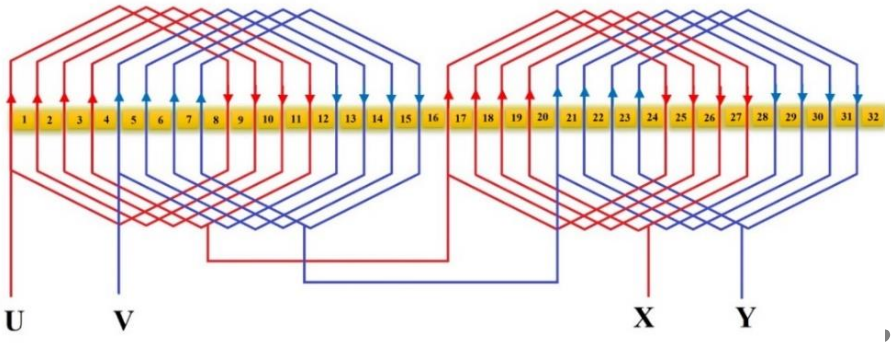

a)

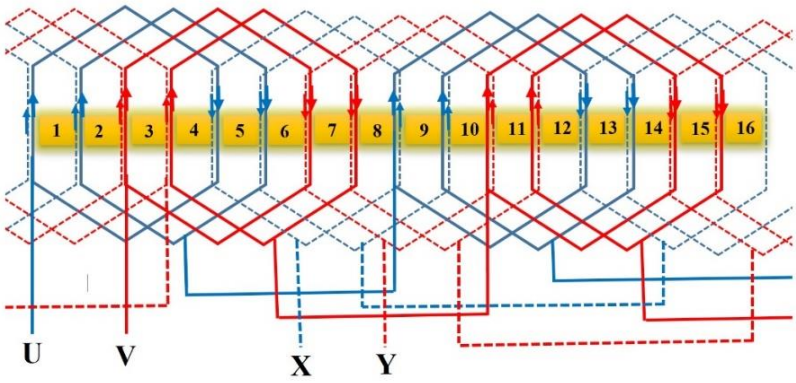

b)

Figure 3: Winding patterns of the proposed resolver: a) Single layer b) Double layer.

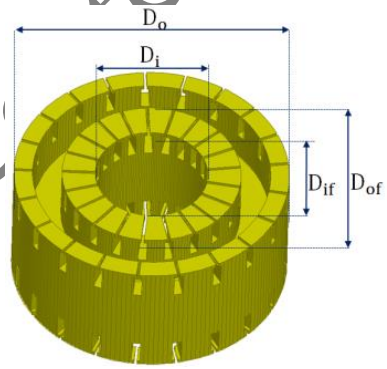

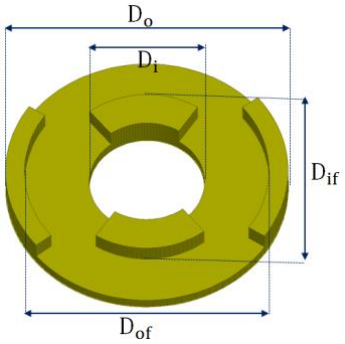

(a) (b)

Figure.4: 3D views of (a) stator and (b) rotor of AFCPR

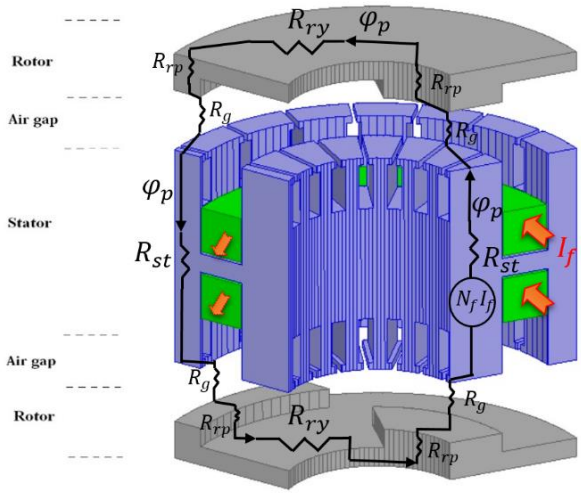

Figure 5: the 3D magnetic equivalent circuit of the pole pair of AFCPR.

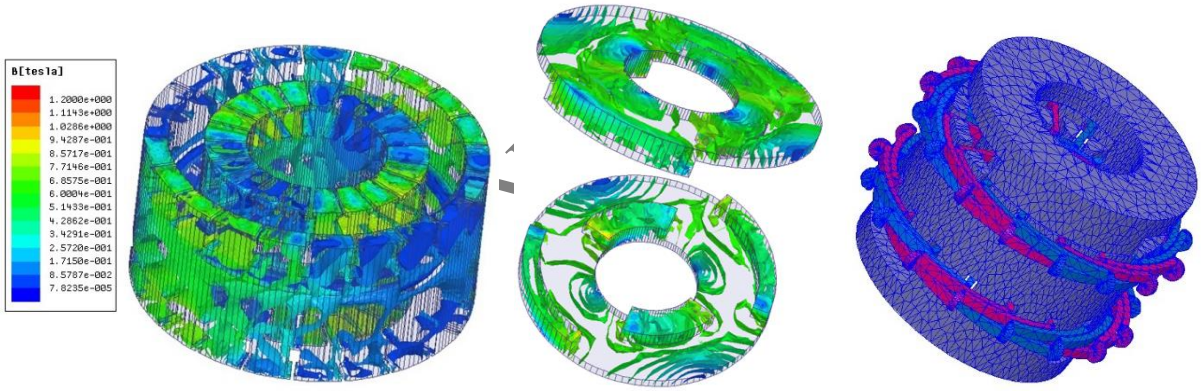

(a) (b) (c)

Figure 6: the magnetic flux density distribution for (a) stator (b) rotor and (c) plot mesh

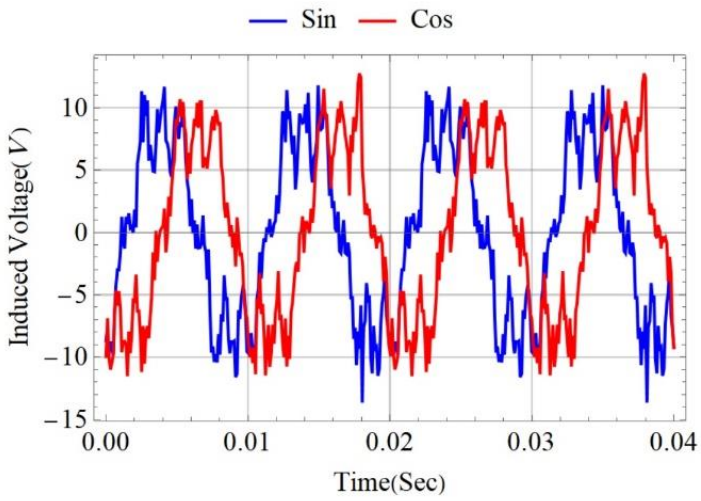

Figure 7: Induced Cosine and Sine voltages of AFCPR with single-layer winding.

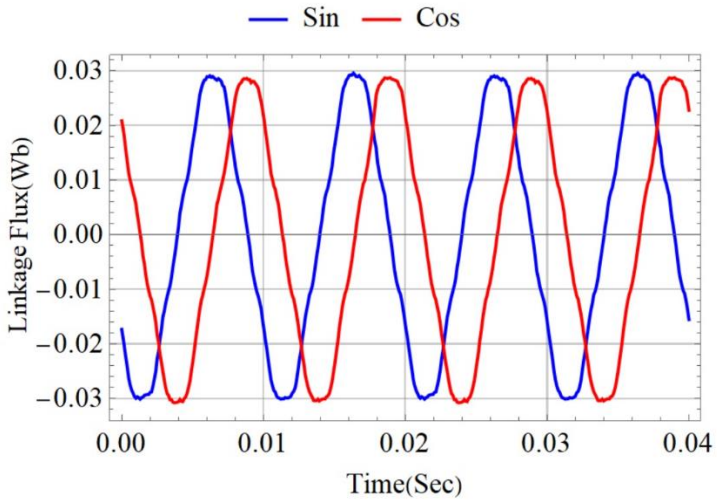

Figure 8: linkage flux profiles of the AFCPR with single-layer winding.

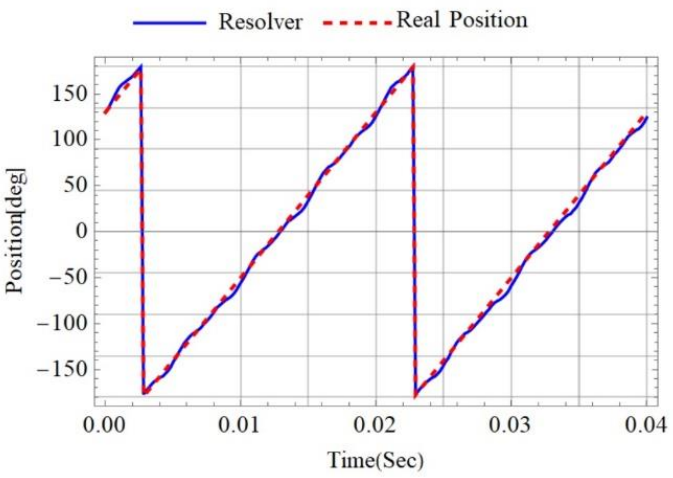

Figure 9: The rotor position estimation $\theta_r(t)$ by the AFCPR compared to the actual rotor position for the single-layer.

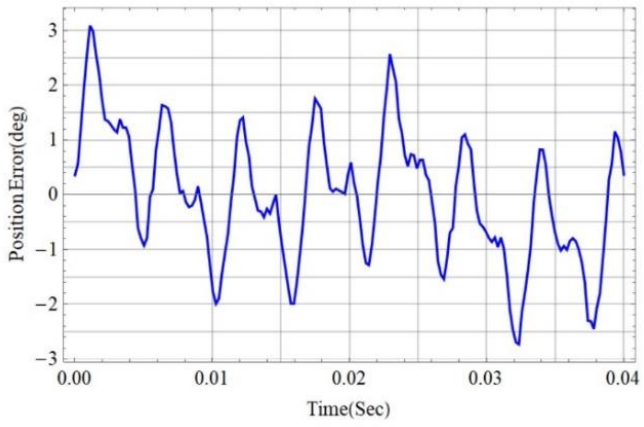

a)

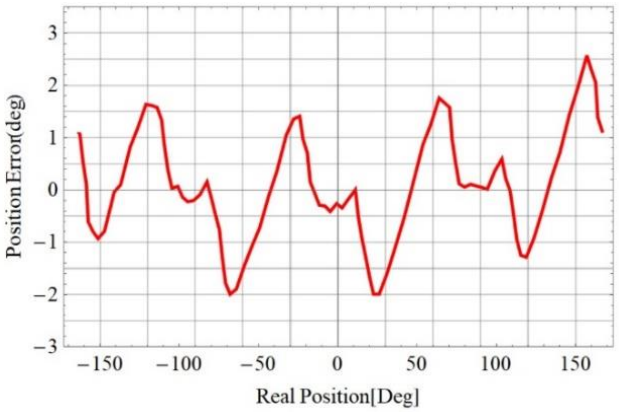

b)

Figure 10: The rotor position estimation error by the single-layer AFCPR as a function of a) time and b) actual position.

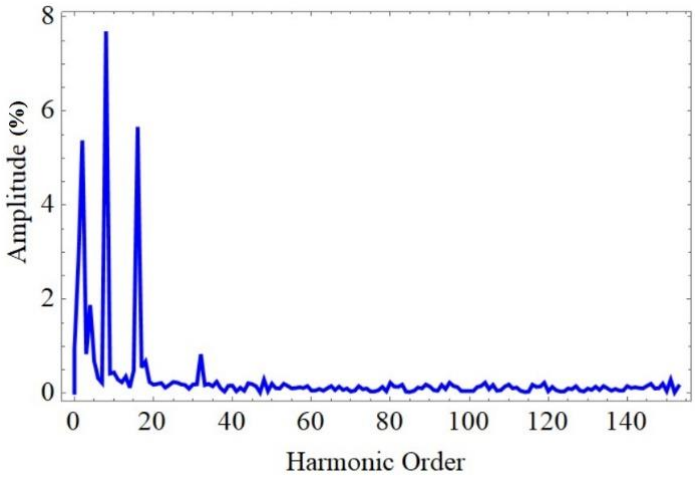

Figure 11: The harmonic content of the rotor position error envelopes for single-layer AFCPR.

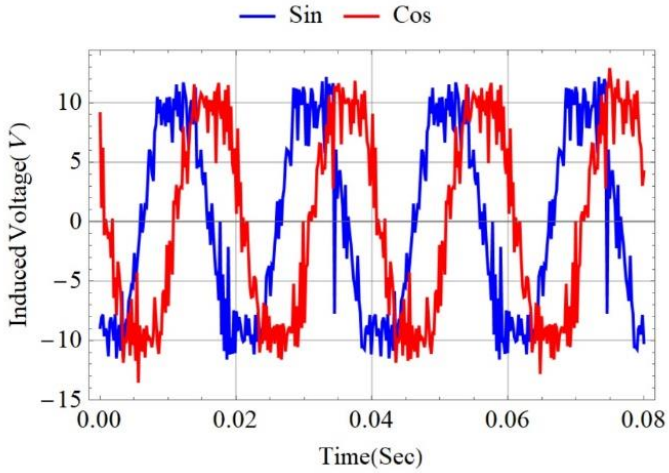

Figure 12: Induced cosine and sine voltages of the resolver windings with double-layer winding configuration.

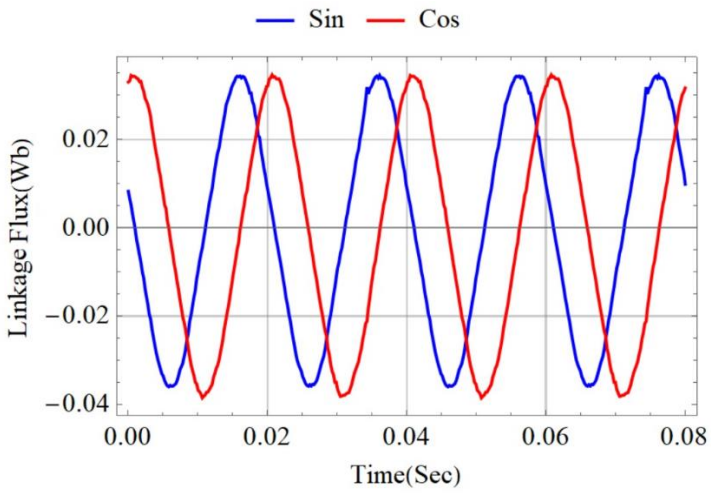

Figure 13: Flux linkage diagrams of the resolver windings with double-layer winding configuration.

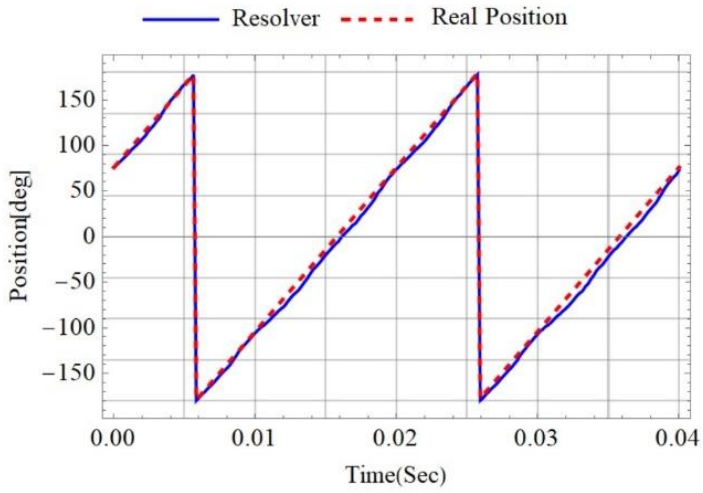

Figure 14: Identified rotor position, $\theta_r(t)$, by the double-layer resolver compared to the actual rotor position.

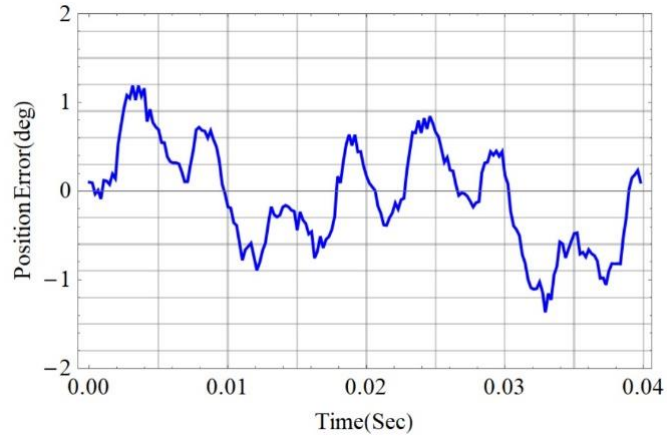

a)

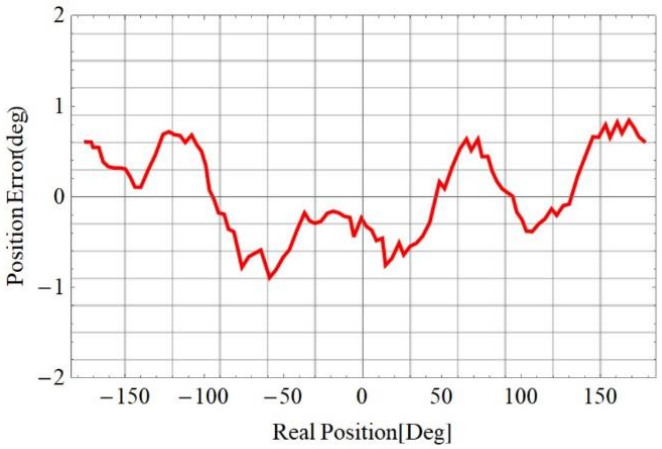

b)

Figure 15: the rotor position estimation error by AFCPR as a function of a) time and b) actual position of the double-layerresolver.

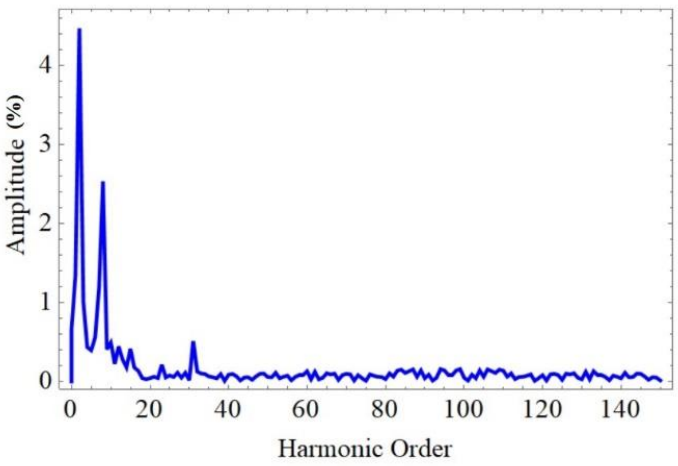

Figure 16: The harmonic content of the rotor position error envelopes for single-layer AFCPR.

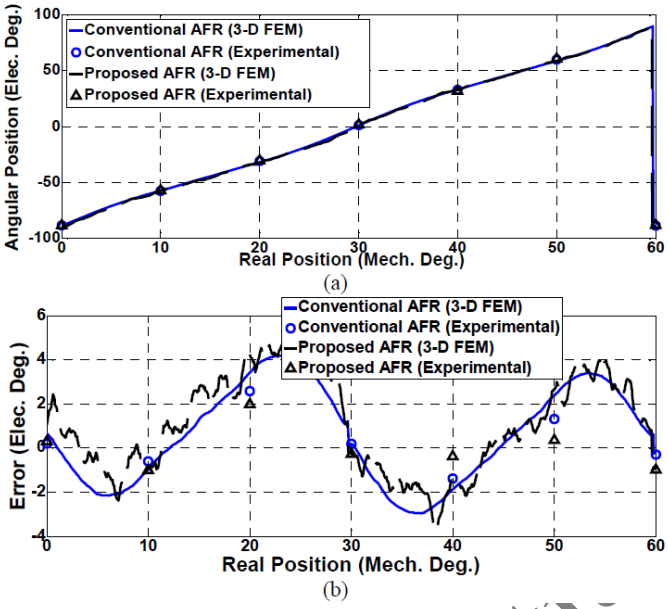

Figure 17: Experimental results of the AFRs presented in reference [27], (a) the detected position versus the reference position and (b) the angular position error